Delfly Flex: a flapping wing micro air vehicle with a bio-inspired unibody composed of compliant joints

Bioinspiration & Biomimetics

OPEN ACCESS

RECEIVED
12 December 2025

REVISED
16 March 2026

ACCEPTED FOR PUBLICATION
10 April 2026

PUBLISHED
8 May 2026

PAPER

Delfly Flex: a flapping wing micro air vehicle with a bio-inspired unibody composed of compliant joints

Sunyi Wang[1], **Martijn den Hoed**[1] **and Salua Hamaza**[*]

Department of Control & Operations, Faculty of Aerospace Engineering, TU Delft, Delft, The Netherlands
[1] These authors contributed equally to the work.
[*] Author to whom any correspondence should be addressed.

E-mail: s.hamaza@tudelft.nl

Keywords: biologically inspired aerial robots, embodied intelligence, compliant mechanisms, flapping wing micro air vehicle, resin 3D printing, soft robotics

Supplementary material for this article is available online

Abstract

Flying insects' thorax houses the flight muscles that provide efficient, multi-axis wing actuation. Such bio-inspiration is essential for developing future flapping wing micro air vehicles (FWMAVs) that combine advanced maneuverability with design simplicity, low weight, and high power efficiency. In this work, we propose a novel unibody with distributed compliant joints inspired by the multiple degrees of actuation freedom of an insect thorax—in particular, wing stroke plane modulation for active pitch and yaw—yielding a compact multifunctional structural component for the 24.6 g FWMAV: *Delfly Flex*. All of these functions are achieved within a single 3.73 g 3D-printed integrated airframe. To design this unibody, we provide an analytical framework that guides compliant joint geometry using differential flexure beam analysis, along with an optimal joint orientation analysis for seamless integration into the unibody. To ensure sufficient structural endurance, we investigate various resin materials and printing configurations, resulting in a robust resin-printed unibody that incorporates two compliant joints and wing-root stabilizers. This single structure replaces the conventional multi-component FWMAV body composed of rigid-hinge-based dihedral pitch & yaw mechanisms attached to a rod-like fuselage. We characterize the flight capabilities of *Delfly Flex* through tethered experiments measuring force and moment generation. The results show thrust generation and yaw moment arms equivalent to its predecessor, while the pitch moment arm is approximately 50% smaller due to the concentrated mass distribution inherent to the unibody design. Free-flight experiments further validate the concept, demonstrating controlled pitch and yaw maneuvers enabled by compliant beams as thin as 0.4 mm. Combined with simplified assembly and more than 10% mass reduction, this unibody concept opens pathways toward future designs with increased deformability and expanded control authority. Overall, this study highlights the synergy between aero-mechanical design and additive manufacturing, achieving enhanced body intelligence through insect-thorax-inspired FWMAV structures.

1. Introduction

The motivation to mimic the flight capabilities of animal flyers has inspired numerous engineering innovations throughout history. Among these, the development of flapping wing micro air vehicles (FWMAVs) stands out as a rapidly advancing research field, particularly over the last two decades. The inherent characteristics of being small and lightweight necessitate the exploration of novel design approaches, materials, and fabrication techniques. A significant hurdle in this pursuit lies in achieving efficient energy transmission between actuators and lift-generating surfaces. The components involved often contribute substantially to the overall system mass and face diminished effectiveness due to frictional or

viscous losses, as noted in [1]. Designing a mechanism capable of fully/partially transmitting actuation with varying degrees of wing surface control freedom, while being structurally compact and lightweight, remains a fundamental challenge in the domain of FWMAVs.

In nature, insects leverage the thorax, situated between the head and abdomen as depicted in figure 1(a), to facilitate flight, walking, jumping and other locomotive activities. This thoracic section, connecting to six legs and potentially two pairs of wings, serves a dual purpose of generating wing flapping motion and regulating the multiple rotational degrees of freedom, including wing stroke plane modulation, through the 18–19 pairs of steering muscles [2]. Wing stroke plane modulation is a well-established biological mechanism for flight control. In *Drosophila*, yaw saccades are driven by asymmetric stroke plane shifts between the two wings [3], while symmetric changes in stroke plane orientation are the primary mechanism for pitch torque generation during hovering [4]. At the thorax level, neurogenic steering muscles directly govern stroke plane orientation. Electrical stimulation of specific sclerite-attached muscles has been shown to induce pitch rotations of up to 22° and contra-lateral yaw of up to 17° in a cyborg beetle [5].

In contrast to the fully integrated thoracic structure of insects—capable of muscle-driven flapping and wing-stroke plane rotation—current FWMAVs rely on a more compartmentalized design. This is largely due to the lack of miniaturized, high-energy-density power sources that can be seamlessly integrated into the airframe. As a result, these systems typically assemble multiple discrete components, such as rigid hinges, revolute joints, linkages, gearboxes, and servos, distributed across the robot to achieve the required degrees of freedom for flapping, roll, pitch, and yaw [6–11]. However, this compartmentalization increases assembly complexity, adds weight, and introduces power losses through actuation transmission. Consequently, current designs remain far from achieving a truly integrated, lightweight, and power-efficient thorax-like system.

In the field of FWMAVs, various works have innovated both the flapping mechanism and the wing stroke plane modulation. Methods that incorporate high-input power through elastic elements create resonance at certain frequencies and enable effective flapping motion. Such methods include direct drive mechanisms such as piezoelectrically actuated thorax [12], dielectric elastomer actuators [13, 14], or liquid-amplified dielectric zipping actuators [1]. For deforming or deflecting the wing such that the stroke plane is modulated to generate an active control moment, innovations such as localized partial-actuation and transmission components, including servo-actuated strings [15] and extension springs [16], have emerged to enhance wing actuation freedom and efficiency. While prototypes inspired by the insect thorax have demonstrated improved thrust per input power [17, 18], achieving a truly thoracic muscle-like structure with high flapping frequencies and various degrees of freedom for flight missions remains an unattained goal, especially under the low power consumption constraint, where most direct drive mechanisms require high power inputs.

In the pursuit of a lightweight structure capable of transmitting motion with specific degrees of actuation freedom, we draw inspiration from the field of compliant mechanisms, where force and motion are transmitted through elastic body deformation [19]. The development of compliant mechanisms for additional task assistance has gained momentum in the soft robotics field [20] and has been integrated into more conventional MAVs. Notably, quadcopters utilize compliant mechanisms for tasks such as perching upon landing [21] and aerial grasping [22, 23]. Fixed-wing MAVs incorporate compliant deployable wings [24] to save space and enhance manufacturability. In FWMAVs, compliant mechanisms capable of flapping, twisting, and swinging motion [25] have also shown potential to provide more repeatable flapping trajectory and reduce the input power due to the store-and-release of strain energy in the compliant beams [26, 27]. A thorax-inspired compliant mechanism designed to generate flapping motion has been manufactured earlier [28], but has never been assembled on a flying platform for validation. Onto a full-scale FWMAV level, the Harvard Robobee provides stroke plane modulation through wing twisting via two orthogonal piezoelectric actuators bridged by a planar compliant hinge mechanism [29]; however, this milligram-scale, piezoelectric-driven approach employing 2D planar hinges is not directly applicable to 25 g-class FWMAVs, which require three-dimensional structural support and mechanically-driven compliant joints (see section 2.1 for a detailed comparison).

Despite previous efforts, a compact and unified assembly capable of both flapping motion and wing stroke plane modulation for larger FWMAVs has yet to be developed to closely mimic natural flyers [30]. This limitation is attributed to challenges in existing power sources, materials, fabrication techniques, and control strategies, preventing the sustained free flight of MAVs relying solely on compliant mechanism actuation.

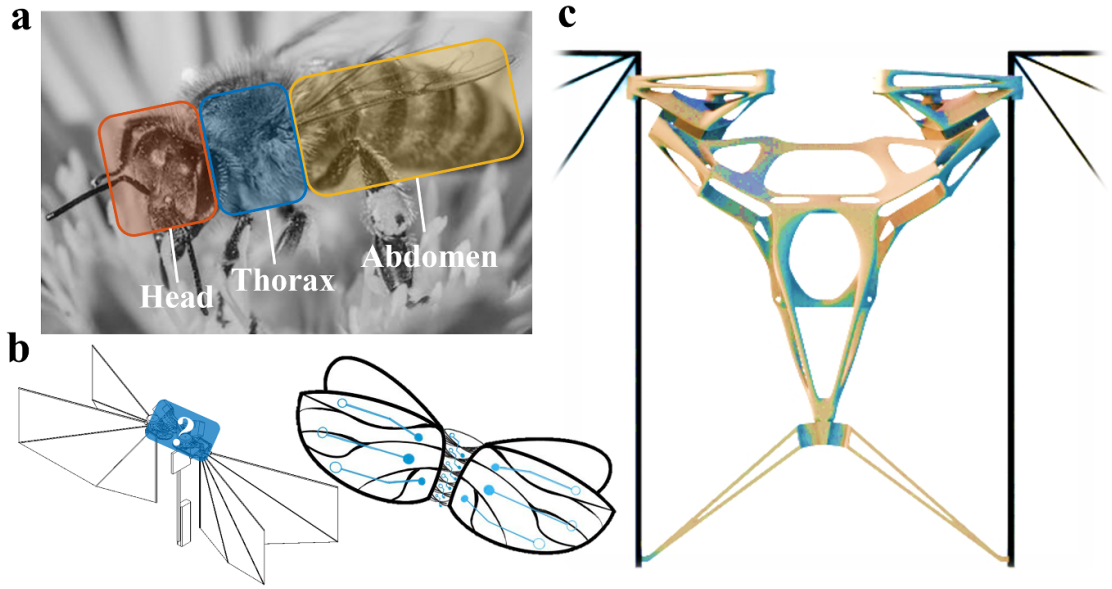

Figure 1. (a) The three main parts of the insect body, with a bee as an example in the background (free stock image from *pexels.com*); (b) a concept evolution of a more integrated bionic FWMAV body; (c) front view of the novel Delfly Flex's unibody rendered in CAD software.

In this work, we present the 24.6 g *Delfly Flex* (shown in figure 1(c)) as the successor of the Delfly Nimble [7], with a unibody that entirely replaces the conventional airframe made of discrete structural components. The FWMAV unibody has an upper body composed of two distributed compliant joints and a lower body housing the major electronics, while providing wing root stabilization through two arm-like rigid beams with semi-rigid hinges. Each compliant joint is composed of 3 cross-pivot flexure beams that actuate either side of the wing pair with coupled swinging and twisting motions.

A practical airworthiness-oriented approach is adopted: the design solution is reached through an iterative process combining analytical compln 2.3), CAD design using spline-based surfaces to minimize local stress concentrations, rapid resin 3D printing, and hover flight validation. No topology optimization is employed; instead, dimensional design is guided by analytical stress and buckling bounds (section 2.3) and refined through flapping durability tests. With the current design, the predecessor Delfly Nimble's gearbox, separate dihedral pitch and yaw control, and the carbon fuselage rod are completely replaced by one unibody with two compliant joints that provide both pitch and yaw actuation in one structure, and a wing stabilizing arm to aid overall flight stability. The life-like, high-quality, low-cost 3D-printed unibody is a highly articulated and functional monolithic structural component that meets the stringent restrictions of the FWMAV platform. It also possesses adequate material strength to withstand hours of operational cycles while maintaining inherent flexibility to facilitate pitch- and yaw-related deformations. During this process of mimicking the thorax's ability for wing stroke plane modulation, we not only make a step further for integrated and multifunctional MAV design (figure 1(b)), but also develop a modeling, design, and fabrication framework that is easily transferable to other areas of miniaturized robotics R&D, using compliant mechanisms and advanced additive manufacturing.

2. Design and analysis

2.1. Flexure selection

In order to provide sufficient elastic body deformation and satisfy the design goal of a muscle-like compliant torso that can accommodate wing flapping motion, the first step is to select compliant flexure designs that have one compliant degree of freedom and can be integrated with the rotatory servo's motion during actuation. Several compliant flexure designs have been considered, including traditional *living* hinges, split tube flexures, butterfly flexures, cartwheel pivots, and cross pivots [31, 32].

As a large range of actuation is desired for sufficient pitch and yaw on Delfly Flex, the living hinge and cartwheel pivot-type mechanisms are deemed inadequate due to relatively high stiffness and limited rotation capability. The butterfly flexure, known for its relatively large range of movement, is considered unfit due to the need for support material when printed in a non-planar orientation—which proved difficult to remove in a clean way, after resin printing. With these considerations, the cross-pivot flexure is chosen as the main mechanism for the wing steering, with the advantages of providing a sufficiently large range of actuation and good spatial accessibility, allowing for easy support removal post resin printing

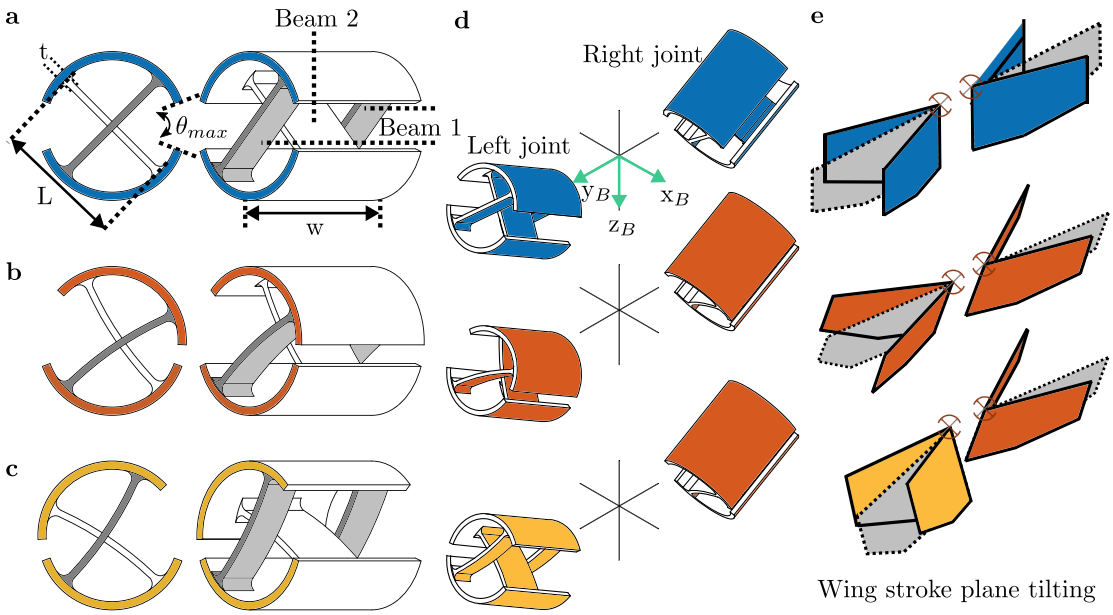

Figure 2. (a) Design parameters of the cross-pivot flexure beams inside one compliant joint of Delfly Flex, with actuation angle θ, flexure beam thickness t, and flexure beam length L. The side view (left) and angled view (right) show two smaller beams (Beam 1, in gray) and one larger beam (Beam 2). The entire joint is shown in its non-deflected neutral state (i.e. producing zero pitch or yaw moment), colored in blue. (b) and (c) Side and angled views of a compliant joint in deflected states, illustrating motion in either direction. (d) Actuation modes using two compliant joints shown in neutral (blue), pitch (red), and yaw (yellow–red pair) configurations. The coordinate system, marked in green, corresponds to the intended body-frame reference of the flapping wing platform. (e) A conceptual view of two compliant joints (in burgundy) embedded in the left and right flapping wing pairs, realizing the wing stroke plane (in gray) modulation. See system-level full assembly in figure 6 and refer to supplementary animation video S1 to understand more visually the motion train from the flexures to their functions in the entire flapping wing platform.

and visual inspection. Unlike the 2D planar compliant hinges used in milligram-scale platforms such as the Harvard Robobee [29], the cross-pivot arrangement provides three-dimensional structural support suited to the 25 g-class X-wing typed FWMAVs, where the biplane layout requires sufficient out-of-plane stiffness to maintain stable and repeatable flapping cycles.

2.2. Differential flexure beam analysis

Once the cross-pivot flexure mechanism is selected, each flexure is connected via a half-cylinder-like casing and a pair of them can be further linked to the flapping wings, and depending on the direction of actuation, the elastic deformation of the beams enables the pitch and yaw motion through the following motion transmission chain: servo arm rotation (which rotates the compliant joint casing) $\rightarrow$ flexure beam bending (due to the joint casing rotating) $\rightarrow$ rotation of the wing stroke plane (as illustrated in figure 2). Specifically, when the servo arm rotates, it applies a moment at the actuation point (illustrated in figure 6(a) of the compliant joint. This bends the cross-pivot flexure beams, and the resulting deformation rotates the portion of the unibody connected to the flapping wing pair about the joint axis J_z, thereby tilting the wing stroke plane. This single-degree-of-freedom pivot allows for low stiffness and large stroke actuation along its longitudinal axis, while achieving high stiffness on the other axes, with relatively low parasitic movement of the pivot point [33].

An analytical characterization of the stresses present in cross-pivot flexure is performed by means of linearized bending stress and static force analysis. Normal stresses due to bending are determined using equation (1), a formula derived from the linear Euler–Bernoulli beam theory, with the following input parameters: actuation angle θ, elastic modulus E, flexure beam thickness t, and flexure beam length L. Normal stresses induced by thrust generated by the wings are calculated using equation (2), with input parameters: flexure beam width w and peak thrust force F, with the assumption of a sinusoidal thrust profile. Last, normal stresses due to off-center positioning of the thrust generated by the wings are calculated using equation (3), with parameter M being the peak moment induced by the wings at the center of the flexure.

$$\sigma_{\text{bend}} = \frac{\theta E t}{2L} \tag{1}$$

$$\sigma_{\text{normal}} = \frac{w * t}{F_{\text{normal}}} \tag{2}$$

$$\sigma_{\text{moment}} = \frac{M}{2tw^2} \tag{3}$$

$$\sigma_{\text{total}} = |\sigma_{\text{bend}}| + |\sigma_{\text{normal}}| + |\sigma_{\text{moment}}|. \tag{4}$$

The summations of the aforementioned stresses, as formulated in equation (4), result in the maximum experienced normal stress of the mechanism. At the

Table 1. Specifications of the compliant flexural and torsional mechanisms.

	Beam 1	Beam 2
Length L (mm)	8.0	8.0
Thickness t (mm)	0.40	0.40
Width w (mm)	2.5	5.0

given scale, stress due to bending of the joint is the major contributor, and results in an upper bound to the thickness of the flexure beam elements. The lower bound of this thickness is determined by the buckling load, such that the mechanism will resist buckling under the forces that are expected during flight. Equation (5) is used to characterize this, derived from the Euler Buckling equation with fixed ends [33]. Complying with this lower and upper bound, a beam configuration is narrowed down and selected after multiple iterations with the help of flapping tests, with its dimensions shown in table 1.

This configuration has a torsional stiffness characterized by equation (6) [33]. The rotary servos must overcome this stiffness throughout the required actuation range; specifically, the servomotors' torque must exceed the moment generated by the cross-pivot flexure at its maximum deflection.

$$F_{\text{buckle}} = \frac{\pi^2 E w t^3}{6L^2} \tag{5}$$

$$K_{\text{pivot}} = \frac{E w t^3}{12L}. \tag{6}$$

2.3. System-level modeling and analytical study

The structural assembly of the compliant torso consists of the gearbox-like support structure (to which the compliant joints are connected), the servo and motor mounts, and the center frame that forms the main airframe linking the wings. To integrate these components into a single continuous unibody structure as illustrated in figure 1(c), the junction regions interfacing different sub-structures are modeled using spline surfaces. To reduce mechanical stress, features with rounded corners at transition regions are used throughout the unibody CAD design. To reduce mass, parts of the unibody are hollowed out maximally wherever some mass can be taken out without jeopardizing structural integrity. Overall, such a CAD modeling approach minimizes surface discontinuities and local stress concentrations, helping prevent the brittle fractures typically observed in resin materials and ensuring sufficient durability over thousands of flapping cycles.

The torso is comprised of three discrete subsystems, which have been modeled individually and combined together in CAD design (figure 3(a1) and more details in figure 6(b)), those being: the compliant joints, the gearbox frames (providing structure for the motors, the gear-crank mechanisms, and connections to the compliant joints), and the centerconnecting structure (top part of the airframe, supporting the servos and housing the electronics). Starting with the gearbox frames, the gear configuration used in Delfly Nimble has been adapted to fit into a smaller, more compact footprint, by rotating the entire subsystem 90° inwards, around the wing pivot. From this gear configuration, the gearbox structure is designed as a set of spline surfaces connecting the axle holes of the gears and support structure for the BLDC motor.

Next, the compliant cross pivot in the joint is designed using conventional, parametric CAD techniques, and then combined with the gearbox frames. Last, the center connecting structure is modeled as a set of spline surfaces, connecting the stationary sides of the compliant pivots to the central structure, whilst also providing a mounting point for the servomotors via a metal pin. A motion study has been performed to verify that the full range of actuation could be achieved without parts interfering, after which it is printed and physically test-fitted with the components, ensuring ease of access for assembly as well.

During the system-level modeling and test-printing process, the question arose of how to orient the compliant joints within the unibody structure. To address this analytically, we compute the pitch moment per unit force generated by the right wing during pitch actuation. During flapping, thrust is produced along the $-z_B$ direction, and the thrust force $\vec{T}$ is represented using a unit vector $\hat{z_B}$ (equation (8)). The location of this force is approximated by the center of pressure (CP), taken to be at 60% of the wingspan near the leading edge. Although the CP shifts dynamically over the wing during a flap cycle [34], this approximation is sufficient for an order-of-magnitude calculation.

Pitch motion is achieved by rotating the right compliant joint by an angle Θ about its joint axis $J_z{}'$. Because the right wing is connected to this joint through the gearbox within the unibody, the entire wing rotates about $J_z{}'$. The moment arm is computed as the vector sum of the vertical offset from the center of gravity (CG) and the horizontal offset from the

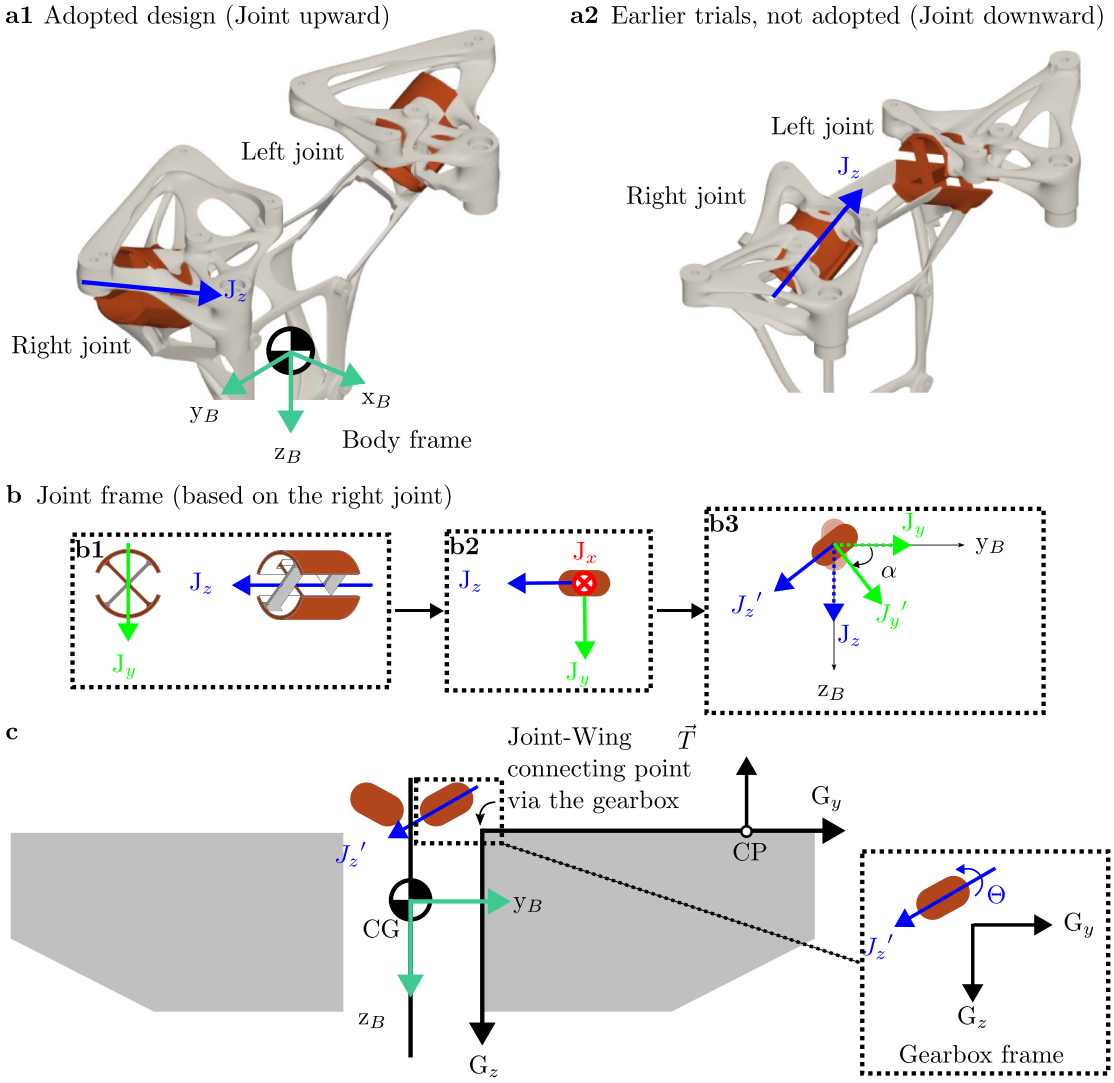

Figure 3. (a1) and (a2) The placements of the left and right compliant joints are shown, highlighting the upward and downward joint orientations considered during design iterations. (b1) Frame of reference J for the right compliant joint, where the J_z axis represents the rotational axis about which the cross-pivot flexure beams deflect. (b2) and (b3) The compliant joint is simplified to a 2D representation and aligned with the body-frame orientation, where α denotes the rotated joint angle and $J_z{}'$ is the resulting joint central axis. (c) A simplified illustration of the Delfly Flex's gearbox configuration relative to the full flapping-wing platform. The gearbox connects the compliant joint to the carbon rod at the wing's leading edge, where a simplified center of pressure (CP) is also indicated. When the compliant joint rotates about the $J_z{}'$ axis by an angle Θ, the entire wing rotates accordingly around $J_z{}'$.

gearbox to the CP (i.e. the dihedral arm and a portion of the wingspan), as expressed in equation (7) and illustrated in figure 3(c).

The orientation of the $J_z{}'$ axis depends on whether the joint is angled upward ($+\alpha$) or downward ($-\alpha$), as shown in figures 3(a1), (a2) and (b3). By varying α, figure 4(derived from equation (9)) demonstrates that an upward-oriented joint consistently produces a larger pitch moment per unit force. This occurs because the wing's rotation/twist axis is directed upward, causing the effective CP location to move dynamically farther from the CG, resulting in greater pitch authority for the upward configuration.

Based on these findings and other practical considerations on structural compactness, mass distribution, and assembly accessibility, we select $\alpha = 60°$ for the final design.

$$\vec{r} = d_z \cdot \left(-\hat{z}_B\right) + \left(d_{\text{dihedral arm}} + L_{\text{wing@LE}} \cdot d_{\text{CP}}\right) \cdot \hat{G}_y \tag{7}$$

$$\vec{T} = -\hat{z_B} \tag{8}$$

$$M_{\text{pitch}} = \left(\vec{r} \times \vec{T}\right) \cdot \hat{y_B}. \tag{9}$$

3. Materials and methods

3.1. Fabrication: resin selection

The compliant torso composed of the compliant joints has been printed using an AnyCubic Photon resin 3D printer, with the *Siraya Fast Mecha White* resin, allowing for rapid and relatively inexpensive iteration (<24 h per iteration cycle) of highly articulated and precise components. Several

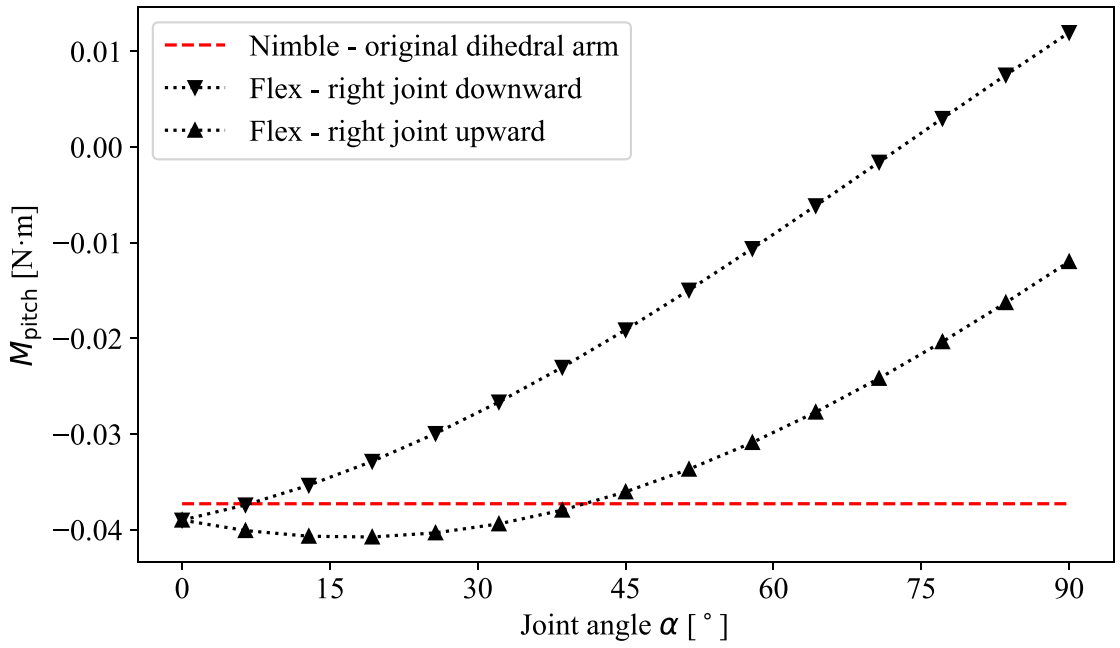

Figure 4. Pitch moment ballpark calculation of the right compliant joint configured upward or downward; the right wing is rotated forward ($+x_B$ direction) 20° via the compliant joint rotating around $J_z{}'$ axis.

Table 2. Mechanical and material properties of different types of resin experimented with (Note: data is chosen for resin in cured state, in *XY* plane; only publicly available information from the technical datasheets is summarized here).

	Flexural (MPa)		Tensile (MPa)			
Used resin name	Strength	Modulus	Strength	Modulus (Young's)	Elongation (%)	Hardness (Shore)
Prusament tough [36]	33.5 ± 2.3	1110 ± 90	41.6 ± 3.7	1600 ± 100	5.8 ± 1.2	75.7 ± 1.2(D)
Self-mixed: 40% prusa tough, 60% photocentric flexible[a] [37]	—	—	4.9	—	—	85(A)
Self-mixed: 20% prusa tough, 80% Zortrax flexible[a] [38]	—	—	7.16	39	19	60(D)
Siraya fast mecha [39]	—	1300	30	1050	6	70(D)
Anycubic colored UV [40]	—	—	45 ± 5	1700 ± 100	14 ± 2	85 ± 1(D)
Phrozen tough abs-like [41]	80	1900	35.8	2200	17.7	77.5 ± 2.5(D)

[a] Only the properties of the second resin used in the mixture are displayed here.

other types of commercial off-the-shelf resin have been used and trialed during the prototyping phase (table 2). However, they all have failed to provide the sought-after balance between rigidity and elasticity, let alone durability in flight testing.

The Siraya Fast Mecha White resin is a composite resin and has the properties of having a hard surface finish and low surface friction, with a higher strength than regular consumer-grade resins, thus suitable for satisfying the need of load bearing during compliant mechanism deformation while being lightweight and durable for an FWMAV. However, during the fabrication process, we have also observed that due to its composite nature with filler particles suspended in the liquid resin for improved mechanical performance, there comes the cost of a slight reduction in dimensional accuracy due to light scattering on the particles, which has also been reported by other users in the community [35]. This light scattering effect inflates the printed components by about 100 μm in the *XY* (horizontal) plane, but does not affect accuracy in the vertical printing dimension. To counteract this effect, a software filter is applied to the 3D files before printing, shrinking the *XY* layers by 100 μm. Furthermore, critical dimensions, such as axle holes and bearing fittings, are drilled out manually post-printing to ensure a perfect tight fit. A layer height of 0.05mm and an exposure time of 11 s have been used, with an off-time of 20 s to allow the resin to settle in between exposure cycles (table 3). Further post-processing steps after printing are: ultrasonic cleaning in isopropyl alcohol, UV post-curing in a UV-curing station, and manual removal of support structures.

3.2. Two possible compliant joint integrations

As the major part of the FWMAV unibody, the designed and manufactured compliant joints can be

Table 3. Resin printer initial settings and fine-tuned settings.

Layer thickness (mm)	Normal exposure time (s)	Off time (s)	Bottom exposure time (s)	Bottom layers	Anti-alias	*Z* lift distance (mm)	*Z* lift speed (mm s^{-1})	*Z* retract speed (mm s^{-1})
0.05[a]	8	1	60	3	1	6	3	3
0.05[b]	11	20	60	3	1	6	3	3

[a] Initial setting; with 5 min curing at mode A (Curing station with internal UV lamp and an automatic rotating platform).
[b] Final setting; with 5 min curing at mode A.

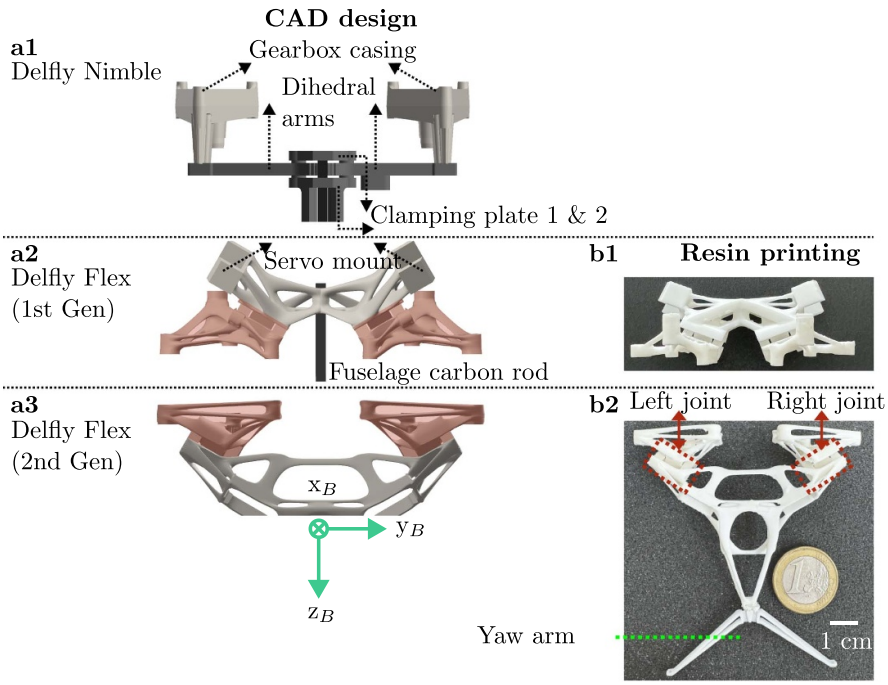

Figure 5. (a1)–(a3) CAD design rendered for Delfly Nimble and two iterations of Delfly Flex, with the 'thorax' region of the FWMAV displayed, and the part of the unibody that would move to rotate the flapping wing pairs highlighted in red; (b1) front view of the resin-printed compliant torso (2.07–2.72 g during design and fabrication iterations leveraging weight miniaturization and overall structural strength); (b2) front view of the 3.73 g resin-printed unibody (printed in one piece) with the FWMAV body frame of reference illustrated (NED convention used), a one-euro coin is used for size comparison, and the area of the left and right compliant joint and the stabilizing arms needed during yaw maneuvers are highlighted.

seen in figure 5, with a comparison to their predecessor Delfly Nimble. Note that despite the orientation of the compliant joint has been optimized analytically (section 2.3), there are again two possible joint integrations in the unibody, this time in terms of the relative position between the compliant joints and the servo mounts. The servos can be placed either above or underneath the compliant joints, as further illustrated in the full CAD assembly rendering in figure 6. After extensive testing, the full unibody (without a separate carbon rod for the fuselage) design is adopted for Delfly Flex, as the ultimate goal of this research is to push for the miniaturization of flight-capable FWMAVs through fusing structural and actuation-related functional components together.

To reach the design of the final version of Delfly Flex, visual inspection of mechanical failure or weak spots of the unibody after many rounds of flapping tests is used to guide through all design iterations, primarily to help improve the local strengthening of the component as needed, with the current 3.73 g version shown in figure 5(b2). We refer to this process as strengthening the unibody of the FWMAV through exercising (i.e. flapping tests) analogously, without the need to use more advanced modeling or simulation of the complex force generation and interaction of flapping wing aerodynamics to aid the 'anatomical' iteration of the unibody. Each iteration always has the pragmatic end goal of sustaining a free hover flight, meaning maintaining low mass while providing sufficient force and moment.

Thanks to the integrated nature of the unibody that houses the two compliant joints and fine-tuned resin printing material and process, the yaw and pitch actuation mechanism is found to be more consistent in terms of assembly and long-term use, than that of Delfly Nimble's, whose dihedral pitch mechanism and servo-attached yaw arm needs individual components and depends on hot-melt adhesives for the positioning on the fuselage rod(where the pitch

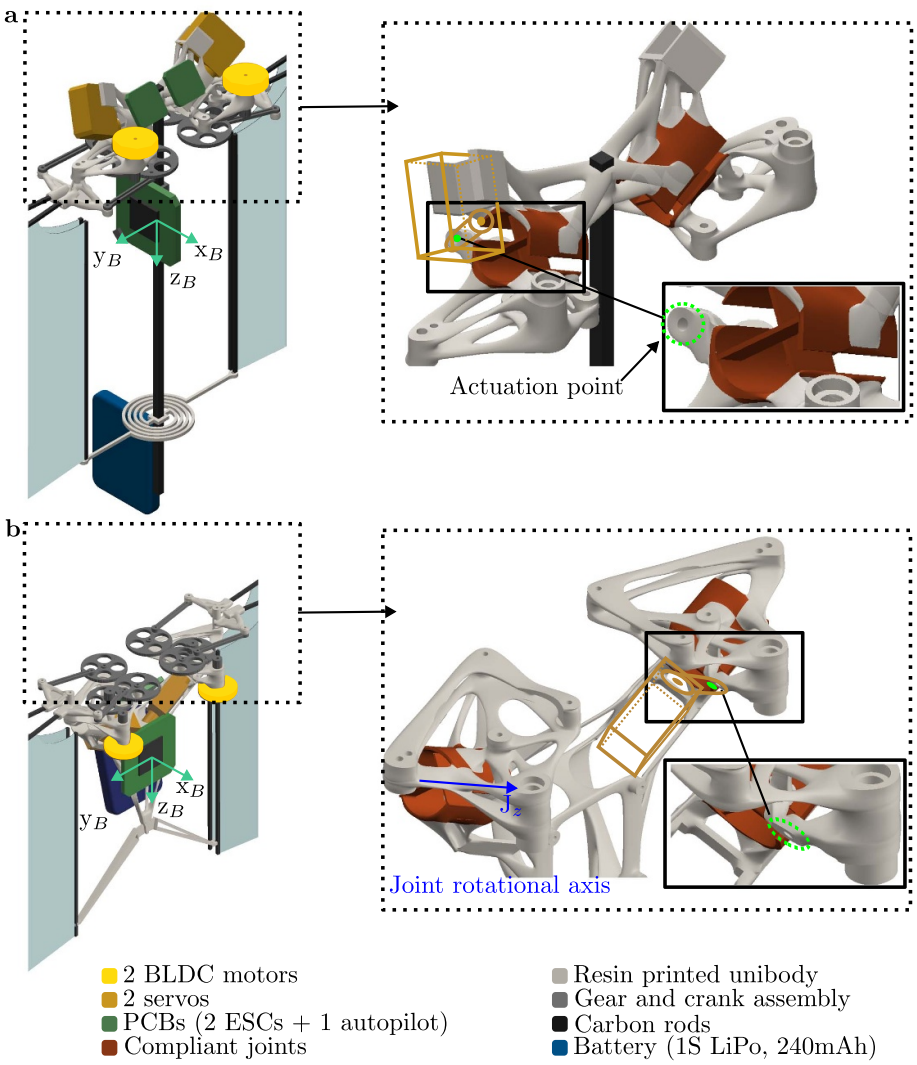

Figure 6. CAD rendering of the entire Delfly Flex 1st generation (a) and 2nd generation (b) (only part of the wingspan shown here), with the compliant joints highlighted in burgundy in particular (See component-level detail in figure 2), and other structures and materials that constitute the FWMAV platform labeled in various colors; in the zoomed-in view on the right, the wireframe view of one servo for actuating one compliant joint is marked in yellow, where the connecting point between the servo arm and the resin-printed unibody (mechanically linked with a metal pin that is not illustrated here) is highlighted in neon green.

mechanism is fixed with two add-on clamping plates as shown in figure 5(a1), and often becomes lose randomly during test campaigns).

3.3. Assembly and control of the Delfly Flex

Contrary to the predecessor Delfly Nimble, where two independent servomotors perform the yaw and pitch control, Delfly Flex utilizes the same two rotary servomotors in a differential setting, each controlling pitch and yaw simultaneously as illustrated in figure 7(a) and demonstrated on the robot in figure 7(b), instead of the linear servomotors used previously on the NUS FWMAV [8] for the similar kind of wing stroke plane modulation. The roll control is maintained similarly, as the embedded gearbox and motor assembly utilize equivalent components and control inputs. The compliant joints undergo an assembly-level optimization in terms of the position and orientation of all the entailed deflection components, to minimize changes in the CG of the FWMAV, and maintain the hoverable state with minimal trimming, ensuring ease of access for manual assembly.

On the Delfly Flex unibody, the actuation and wing assembly on each side can be oriented independently, similar to the mechanism used in tilt-rotor drones. The pivoting joint connecting the gearbox–wing sub-assemblies to the airframe is replaced by a single monolithic flexure, capable of delivering equivalent flight performance and controllability. This design configuration leads to a significant reduction in part count and mechanical backlash, while improving assembly consistency compared to the intricate, manually assembled pitch and yaw joints in the original Delfly Nimble design (figure 6 and table 4). In the previous design, the pitch and yaw mechanism required multiple components, including clamping

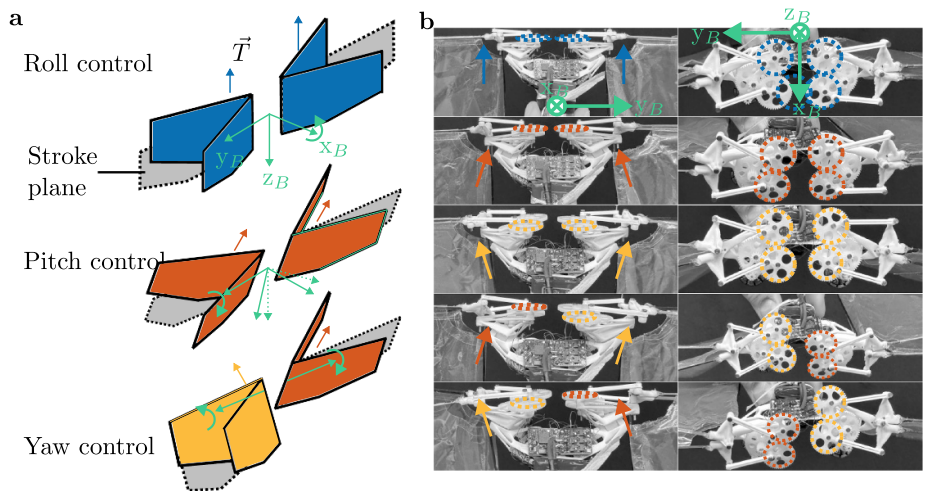

Figure 7. (a) The roll, pitch, and yaw control of Delfly Flex, where the wings in blue indicates the compliant joints are in zero deformation state and only the flapping frequency varies for roll control, the wings in red and yellow indicate opposite joint deformation states, with the same colors indicating pitch motion and the different colors indicating yaw through differential difference; (b) close views of Delfly Flex (left column: front view with x_B axis in the body frame forward, right column top–down view with x_B axis downward and z_B axis to the left) at the states of zero pitch or yaw, pitch forward, pitch backward, yaw clockwise, and yaw counter-clockwise, with an animation that illustrates further in the supplementary video S1.

Table 4. Assembly efforts and parts count.

	Delfly Nimble	Delfly Flex
3D printed/injection molded segments	11	2
Carbon fiber segments	6	2
Metal rods/pins	3	2

Note: Number of parts for actuation excluding the gear train and wing assembly.

plates, servo arms, and dihedral arms, to be manually positioned, bonded, and tightened in precise relative alignment. Reproducing the correct positioning and clamping tension was inherently difficult, particularly during rebuilds, making the process both time-consuming and inconsistent.

The new unibody replaces these assembled interfaces with a single monolithic printed structure, reducing the actuation-related part count from 20 discrete components to 6 and eliminating hinge installation and inter-part alignment steps. Continuous material replaces discrete joints, and flexure-based motion replaces rolling and sliding contacts, thereby removing sources of mechanical play such as dihedral arm tooth clearance, sliding interfaces, and clamped plates that can loosen over time (components labeled in figure 5(a1). This reduces tolerance stack-up and mechanical backlash while ensuring that each rebuild directly reproduces the geometry defined by the printed structure, without requiring manual alignment of internal actuation interfaces.

Beyond transmitting actuation, the compliant joint also redistributes aerodynamic and inertial loads from the flapping wing assembly into the unibody structure. This isolates the servo shaft from multi-directional cyclic loads and improves overall durability. With the latest design iteration, the mass distribution is also more centered around the CG of the robot, resulting in a more compact system architecture.

4. Results

4.1. Tethered flight performance

Both Nimble and Flex undergo three sets of repeated force balance measurements. The drone is mounted on a 6-axis force and torque (F/T) sensor ATI Nano 17 (the titanium version) with a custom-made clamping mechanism that wraps around the fuselage rod near the drone's CG (both the sensor location and CG illustrated in figure 8), with the thrust vector primarily aligned with the $+y$ direction in the ATI coordinate system (denoted in subscript @F/T). After the drone is mounted, an initial calibration to remove all biases is performed before the start of any measurements.

Data acquisition is done with two National Instrument NI 9237 to acquire the differential signals from the F/T sensor, and with data transmission through NI compact RIO controller 9024 with an FPGA module. All measurements are sampled at 10 kHz for 2 s, given the limited data buffer size. The tethered flight is first conducted approximately at the drone's flapping frequency in free-flight hovering,

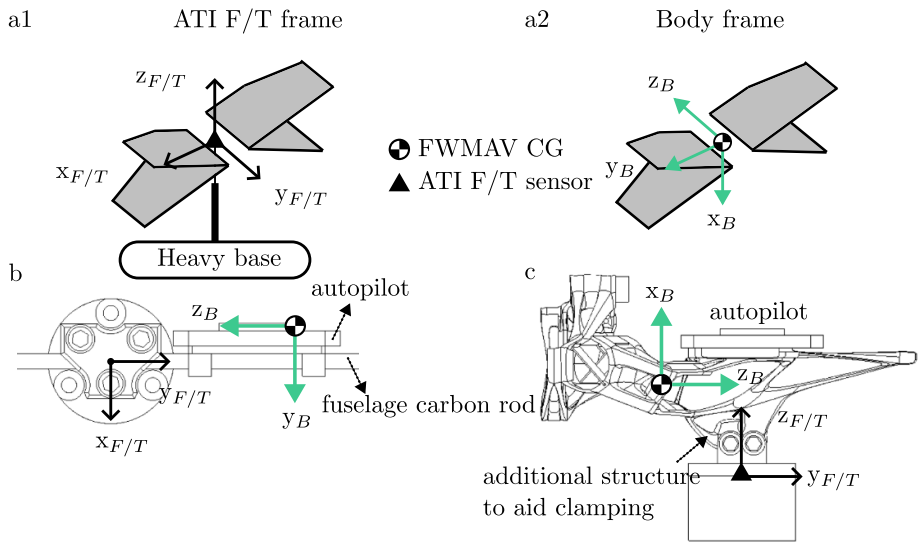

Figure 8. (a1) ATI F/T measurement set-up with its own coordinate system, where the F/T sensor location is marked with a black triangle; (a2) the FWMAV's body frame of reference aligned with the robot's placement onto the ATI system, where the estimated center of gravity (CG) is labeled; (b) Delfly Nimble's fuselage carbon rod being clamped with 3 screws in a clamp plate (3D printed with PLA material) onto the ATI F/T measurement unit; (c) Delfly Flex being fixed onto the ATI F/T measurement unit with additional structural component built into the main resin-printed body frame.

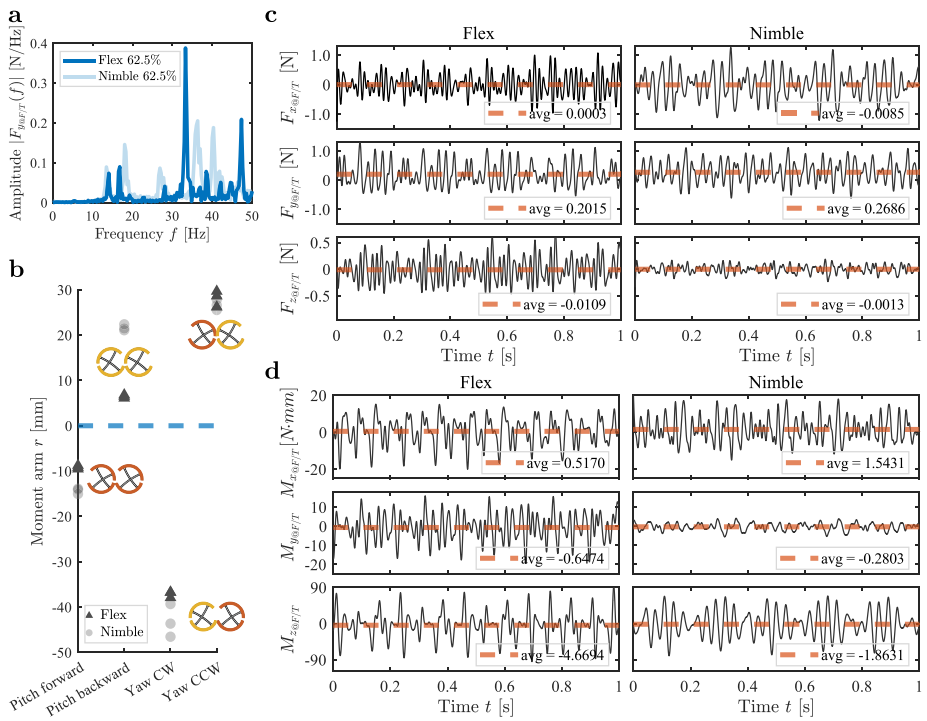

Figure 9. (a) Single-sided frequency spectrum amplitude at hover throttle for both Delfly Flex and Delfly Nimble; (b) pitch and yaw effective moment arm at hover throttle (62.5% command thrust input on the transmitter for a stable manual hovering flight) for both Delfly Flex and Delfly Nimble; (c) and (d) *xyz* direction force and moment generation (in the ATI frame of reference @F/T, illustrated in figure 8) at hover throttle for both Delfly Flex and Delfly Nimble, with the time-averaged value marked in dotted red lines.

which is approximately 17 Hz [7] at around 60%–65% throttle level. The throttle level is configured through the transmitter settings, where an average value of 62.5% is chosen for both robots.

Data processing is performed in MATLAB, with all the force and moment data low-pass filtered by a 4th-order Butterworth filter. Given the indication from figure 9(a), a cutoff frequency of 50 Hz is selected given that the first fundamental frequency of the force F_y (of which the direction is equivalent to the vertical force's in a hovering free flight) and the second harmonics are most likely

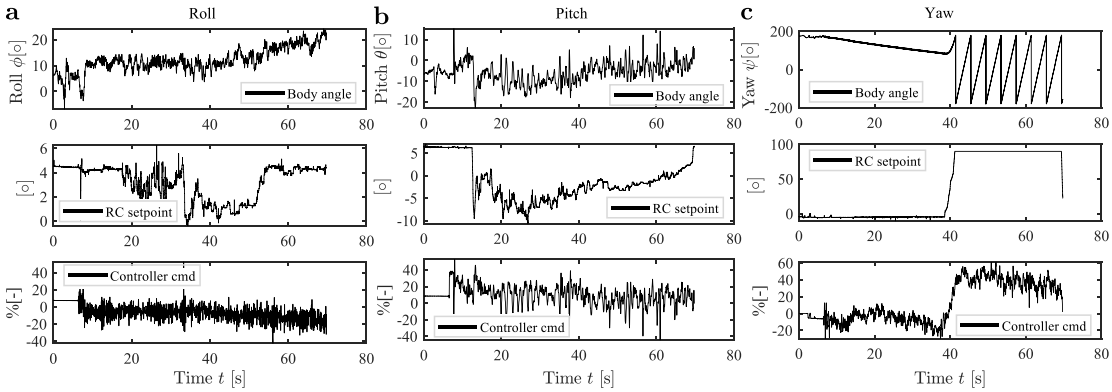

Figure 10. Approximately 70 s of free flight log of Delfly Flex from onboard SD card logging, with first about 30 s of hover, and then yaw clockwise for about 7 full cycles; (a)–(c) show respectively the roll, pitch and yaw in terms of the extent of body angles in the FWMAV's body frame of reference, the RC setpoint from transmitter input, and the percentage from the controller command.

attributed to the aerodynamic force generation while the following up harmonics are more likely attributed to the wing structural mode excitations [42]. The moments recorded in the ATI frame of reference have been transformed to the drone's CG respectively, and are shown in figure 9(d). The pitch and yaw command input is triggered through the transmitter. The measurement is recorded while the maximum pitching forward or backward state, and yawclockwise or counter-clockwise state is being maintained. The recorded data leads to the analysis of effective moment arm analysis (equations (10) and (11)) in figure 9(b),

$$r_{\text{pitch}} = \frac{\overline{M_{x,@F/T}}}{\sqrt{\left(\overline{F_{y,@F/T}}\right)^2 + \left(\overline{F_{z,@F/T}}\right)^2}} \tag{10}$$

$$r_{\text{yaw}} = \frac{\overline{M_{y,@F/T}}}{\sqrt{\left(\overline{F_{x,@F/T}}\right)^2 + \left(\overline{F_{z,@F/T}}\right)^2}}. \tag{11}$$

To prove the sufficient actuation and force transmission of the compliant joints on Delfly Flex, and to compare with its predecessor as a benchmark, we perform both tethered force and moment experiments. Before performing the tethered flight tests, both FWMAVs first undergo a manual hover flight to ensure the proper tuning of the controller gains in the feedback loop for stabilization (For Delfly Flex, see figure 10 as an example of flight log).

The force and moment analysis from one of the repeated tests for each drone at hover throttle in a neutral position (zero pitch or yaw command) are shown in figures 9(c) and (d). A fraction of 50% of the data (recorded in one second) is shown here for better presentation clarity. As depicted in figure 9, both Delfly Nimble and Flex demonstrate the capability to generate a thrust force adequate for sustaining free flight ($F_{y_{@F/T}} > m_{\text{drone}} \cdot g$). In this context, the effective thrust force is assumed to be in the mid-stroke plane of the wing pairs (as illustrated in gray in figure 7(a) and is approximated along the $y_{@F/T}$ direction. The higher magnitude of $F_{y_{@F/T}}$ from Nimble can be attributed to differences in power distribution internally, factory differences in electronics (since the same power supply bench has been used as the power source), or measurement set-up differences due to different clamping mechanisms. The symmetrical flapping motion of the identical wing pairs results in an almost-zero value for the averaged $F_{x_{@F/T}}$ and $F_{z_{@F/T}}$ as forces produced in these directions by each wing pair cancel out during flapping cycles. Thanks to the more compact unibody configuration of Delfly Flex and the integrated clamping mechanism for the tethering to the ATI sensor, it now produces a similar level of vibrations as Delfly Nimble, contrary to its previous iterations.

For both drones, the average effective moment acting on the pitch axis ($M_{x_{@F/T}}$) and yaw axis ($M_{y_{@F/T}}$) is close to zero, reflecting their near-neutral state during flapping to emulate free (untethered) hovering flight around a fixed location. The small non-zero residual moments observed at hover are attributable to minor asymmetries in the manually constructed wings (e.g. slight differences in membrane tension or mass distribution) and small variations in motor performance between the two sides, rather than systematic control offsets. Vibration-induced dynamic coupling within the measurement setup may also contribute. The ATI system is calibrated to zero before each measurement to remove sensor bias. Delfly Flex exhibits a higher average roll ($M_{z_{@F/T}}$) moment, primarily attributed to relatively more vibrations from the top part of the unibody where the compliant joints are housed. The unibody's wing root stabilizing arms have comparable performance as the yaw servo arm that stabilizes the wing roots on Delfly Nimble, since the average yaw ($M_{z_{@F/T}}$) moment is close to zero for both robots. The wing root stabilizing arms play a crucial role in

reducing wing root vibrations without limiting the full range of yaw motion. Due to the lack of the yaw servo constraint on the yaw arm, Delfly Flex theoretically can generate faster yaw motions with a higher yaw rate setpoint and reference generator yaw rate.

To further compare both drones' capabilities while ruling out the mechanical and electrical differences of both robots, we take a look at the effective pitching moment arm at different states, given that the pitch moment generation is the most critical to a MAV's attitude stability and control [43]. As seen in figure 9, due to the much more compact design of the unibody, Delfly Flex's more concentrated mass distribution around its CG leads to a smaller rotational inertia around the pitch axis. This is reflected through the smaller pitch moment arm. With the same yaw rate settings in the controller for both drones, both robots display the same extent of effective yaw moment arm.

4.2. Free flights

The free flight test is performed in the 10 m by 10 m Cyberzoo flight area of TU Delft Aerospace Engineering department. The same cascaded PD controller with attitude feedback from the IMU (onboard the 1.45 g autopilot Lisa MXS) designed for Delfly Nimble is used on Delfly Flex as well. The open source autopilot Paparazzi UAV has been used for flight control, with the `int_euler` stabilization module. The P gain in the pitch feedback loop that enables a stable hovering flight of Delfly Nimble is first adopted and then further tuned from 7800 to 8000. The rest of the feedback loop gains, the angles and rates used in setpoints and reference generators for both robots are kept the same. Only the servos' shaft position range, the motor mixing, and the IMU orientation have been adapted for Delfly Flex's modes of operation. The same batch of Hyperion 180 mAh 25 C one-cell LiPo batteries are used. The hover flight verification is piloted through manual inputs with a DEVO-10 transmitter.

4.3. Discussion

From conceptual design with simplified analytical modeling techniques, to a flight-capable unibody airframe configuration, there are two main challenges. The first one lies in the way of thinking in designing and fabrication. The traditional component-by-component adding approach is more natural and straightforward for assembly, while it is less intuitive to directly go for an integrated approach where the concept of individual components fades, and functions and structures fuse together, where a structural component is no longer only a fixed structural component. Such a design thinking inspired by flying animals' thoracic structures is what motivated this research initially, and proves to be feasible for 30 g level MAVs.

Second, looking for accessible materials and fabrication techniques that can be integrated into a free-flight capable FWMAV has gone through some educated trial-and-error. Although current technology is still far from the organic building blocks of nature, the rapid advancement in accessible resin printing has made our FWMAV's transition from a discrete component-based body to a continuous unibody construction possible.

Once the above two challenges are tackled, the analytical modeling and design optimization (in particular, the compliant joints) needed for sufficient moment generation and flight maneuverability come logically and relatively easily.

The physical intuition that guides all the design iterations is highlighted and further explained here. Figure 7(a) displays Delfly Flex's control through the wing stroke plane rotation. When further decomposed, this wing motion is superimposed by the wing swinging through rotating around the G_z axis and the wing twisting around the G_y axis (figure 3(c)). Meanwhile, Delfly Nimble utilizes only the swinging degree of freedom (by rotating the dihedral arms shown in figure 5(a1) to redirect the thrust vector for pitch moment generation. This implication indicates a coupled pitch and yaw moment generation due to the way the compliant joint is oriented in relation to the pitch or yaw axis. And this joint orientation (which inherently determines the rotational axis of the compliant joint directly) affects the effective pitch moment generation, which is critical for the stabilization and control of the robot.

To further look at the coupled pitch and yaw moment generation, this can have both advantages and disadvantages in FWMAV control. On one hand, through shared pitch and yaw control actuation, the simplified mechanisms could lead to a more weight and size-efficient robot. On the other hand, this could bring cross-coupling effects, where control inputs for one rotational axis limit inputs for the other axis, which leads to reduced control range and stability. The predecessor Delfly Nimble has decoupled mechanisms for pitch and yaw, making pitch and yaw mixing possible. For Delfly Flex, due to the limited extent the compliant joints can deflect, when the FMWAV is at 100% pitch, there is no further deflection space left for yaw, if pitch and yaw need to be mixed for certain maneuverability demands. Vice versa, same for 100% yaw, where no pitch moment would be available. This explains the reduced manual free flight time as shown in figure 10. This is a conscious design choice, as the goal of this research is to mimic the thorax concept mechanically and explore accessible resin printing technology & materials to design a lightweight flight-capable novel 'airframe' that is multifunctional, all in one piece. After demonstrating the design methodology and proof-of-concept free flight, a full quantification and optimization of flight

maneuverability would guide future design work of the compliant joints.

More efforts in compliant mechanisms and flight control design will be needed. Optimizing the compliant mechanism design has been an interesting and computationally challenging research topic in the mechanical engineering community. Linking the structural deformation capability to flight control demand, the range of control for each axis also needs to be examined in more detail. In the end, reaching insect-like miniaturization, agility, maneuverability, and stability will require further system-level design iterations. In the current design, the achieved yaw rates are comparable to those of the predecessor platform, while the achievable pitch range is somewhat reduced owing to the more compact mass distribution of the unibody. Enlarging the effective deflection range of the compliant beams, adjusting the unibody geometry to increase effective moment arms, and tuning joint stiffness are promising directions to increase control authority in future designs.

Last, the other significant design difference from the energy perspective is the servo load alleviation through the flexure beams in the compliant joints, as both the flexures and the servo arms have the elasticity to return to the beams' neutral position. Thus, the potential energy stored in the compliant joints [44] helps reduce the servo load, which is an intrinsic advantage over rigid hinge-based design for the dihedral mechanisms that are linked to the wings directly for all the motions. The servo's active position control additionally suppresses free oscillations of the compliant mechanism. While some additional vibrations are observable in the tethered force measurements (figure 9), particularly in the F_z and M_y components under fixed conditions, no detrimental resonance was observed during free-flight experiments. The stroke-plane modulation operates at a control bandwidth lower than the wingbeat frequency, and deformation speed is governed primarily by the servo rather than the flexure stiffness, which further assists return motions. No deformation-delay-related control limitations were observed in flight tests, indicating sufficient bandwidth for stable and agile flight within the intended flight envelope.

5. Conclusions

In this work, we re-conceptualize the design and fabrication of FWMAVs, departing from the traditional rigid linkage approach used in major actuation units. Inspired by the intricate flight muscles of an insect's thorax, we introduce an approach that fully integrates the compliant body into the drone's airframe. This unibody architecture represents a departure from conventional robot assembly, which typically depends on separate, discrete components. The result is a paradigm shift in FWMAV construction, with benefits extending beyond fabrication into newer strategies that enable actuation and broader functionalities at the same time.

Our simple, yet effective, design and fabrication approach leads to a unibody with compliant beams capable of generating sufficient deflection for reliable pitch and yaw actuation in an FWMAV. Our Delfly Flex demonstrates controlled and repeatable coupling between force and deflection while greatly reducing assembly and maintenance effort (table 4), thanks to the favorable material properties of the resin-printing technique and its minimal fatigue. Although soft, flexible materials are often regarded as unsuitable for load-bearing or actuation transmission, our results show that this approach offers clear advantages for systems with strict size, weight, and power constraints such as FWMAVs, where unconventional solutions are frequently required. While compliant mechanisms exhibit more coupled force–deflection behavior than rigid-body mechanisms, thoughtful mechanism design combined with system-level integration can shift traditionally discrete architectures toward a more continuous, biologically inspired mode of storing and releasing energy [45].

Throughout our work, we demonstrate the successful integration of the compliant joints to mimic the wing stroke plane modulation function of the insect thorax on the FWMAV Delfly Flex. While the compliant mechanism design holds significant potential, its full capabilities can be realized by refining the deformability and range of deflection of the compliant beams, or designing the force-deformation response with certain flight applications in mind. This refinement should be achieved without compromising structural durability. Additionally, improvements in the flight controller design, coupled with further mixing and tuning, are essential to fully exploit the actuation range and responsiveness of the compliant mechanism. This optimization allows us to further benefit from having compliance in mechanical design, resulting in more lightweight, agile, controllable, and maneuverable FWMAVs.

As access to common 3D-printing techniques such as fused deposition modeling and stereolithography (SLA) (both used in this work) continues to expand, this study encourages the robotics community, particularly the MAV field, to consider SLA for fabricating not only structural and mechanical components but also actuation-transmission elements. When combined with compliant design, the expanding range of lightweight, flexible, and durable materials enables functional parts that efficiently convert potential energy into kinetic energy. This capability facilitates more localized actuation and morphological adaptation, supporting the development of robots with multi-modal functionalities.

There is still a long way for next-generation bio-inspired MAVs to have a truly bionic body that is capable of not only actuation but also sensing, load

Table 5. Mass contribution of major components in Delfly Flex and Delfly Nimble.

	Delfly Flex		Delfly Nimble	
Functionality	*Mass (g)*	*% mass in assembly*	*Mass (g)*	*% mass in assembly*
Electronics	8, 3	34, 2	8, 3	33, 7
Structural	4, 5	18, 5	4, 6	18, 8
Propulsion	11, 5	47, 3	11, 7	47, 5
Total	24, 3		24, 6	

The take-off mass for Delfly Flex is approx. 24.6 g, while for Nimble is 26.2 g after we assembled everything with minimal possible materials (including wires, hot glue, and solder tin), and the original Delfly Nimble is 28.2 g [7]. The current data in the table is the mass of each component measured separately and then added together. All the assembly needed add-on materials are not included in these measurements.

bearing, and other muscle-like multi-functionalities. We hope to inspire researchers to experiment in multiple disciplines, bringing together all necessary tools and materials needed to create more resilient, agile, power-efficient, and mission-capable MAVs.

Acknowledgments

The authors would like to thank Dr. Christophe de Wagter for his discussion during testing and writing.

Data availability statement

All data that support the findings of this study are included within the article (and any supplementary files). The raw experimental data that supports figures 9 and 10 have now been open sourced to https://doi.org/10.4121/eee88ebe-739b-4bff-bf4a-4dd248d91eeb.

Funding

No external funding.

Author contributions

Sunyi Wang 0000-0002-7504-4433
Conceptualization (lead), Data curation (lead), Formal analysis (lead), Investigation (equal), Methodology (equal), Project administration (equal), Resources (equal), Software (lead), Supervision (supporting), Validation (lead), Visualization (lead), Writing – original draft (lead), Writing – review & editing (supporting)

Martijn den Hoed 0009-0006-0233-4305
Conceptualization (lead), Data curation (supporting), Formal analysis (equal), Investigation (equal), Methodology (equal), Project administration (supporting), Resources (equal), Software (supporting), Validation (supporting), Visualization (supporting), Writing – original draft (supporting)

Salua Hamaza 0000-0001-5261-2680
Conceptualization (equal), Formal analysis (supporting), Funding acquisition (lead), Investigation (supporting), Methodology (supporting), Project administration (equal), Resources (equal), Supervision (lead), Validation (supporting), Writing – original draft (supporting), Writing – review & editing (lead)

References

[1] Helps T, Romero C, Taghavi M, Conn A T and Rossiter J 2022 *Sci. Robot.* **7** eabi8189
[2] Deora T, Gundiah N and Sane S P 2017 *J. Exp. Biol.* **220** 1382–95
[3] Fry S N, Sayaman R and Dickinson M H 2003 *Science* **300** 495–8
[4] Fry S N, Sayaman R and Dickinson M H 2005 *J. Exp. Biol.* **208** 2303–18
[5] Vo-Doan T T, Dung V T and Sato H 2022 *Cyborg Bionic Syst.* **2022** 9780504
[6] Keennon M, Klingebiel K and Won H 2012 Development of the nano hummingbird: a tailless flapping wing micro air vehicle *50th AIAA Aerospace Sciences Meeting* (AIAA) p 588
[7] Karásek M, Muijres F T, De Wagter C, Remes B D W and De Croon G C H E 2018 *Science* **361** 1089–94
[8] Nguyen Q V and Chan W L 2018 *Bioinspir. Biomim.* **14** 016015
[9] Tu Z, Fei F and Deng X 2020 *IEEE Robot. Autom. Lett.* **5** 4194–201
[10] Phan H V, Aurecianus S, Au T K L, Kang T and Park H C 2020 *IEEE Robot. Autom. Lett.* **5** 5059–66
[11] Hoff J, Jeon N, Li P and Kim J 2021 Bat bot 2.0: bio-inspired anisotropic skin, passive wrist joints and redesigned flapping mechanism *2021 IEEE/RSJ Int. Conf. on Intelligent Robots and Systems (IROS)* (IEEE) pp 8424–30
[12] Sitti M 2003 *IEEE/ASME Trans. Mechatronics* **8** 26–36
[13] Cao C, Burgess S and Conn A T 2019 *Front. Robot. AI* **5** 137
[14] Chen Y, Arase C, Ren Z and Chirarattananon P 2022 *Micromachines* **13** 1136
[15] Olejnik D, Sujit A, Karasek M, Remes B and De Croon G 2018 Wing sweeping mechanism for active control and stabilisation of a flapping wing MAV *10th Int. Micro-Air Vehicles Conf.* pp 120–6
[16] Jeong S H, Kim J H, Choi S I, Park J K and Kang T S 2022 *Biomimetics* **8** 6
[17] Khan Z, Steelman K and Agrawal S 2009 Development of insect thorax based flapping mechanism *Proc. of the 2009 IEEE Int. Conf. on Robotics and Automation* (IEEE) pp 3651–6

[18] Chin Y W and Lau G K 2012 'Clicking' compliant mechanism for flapping-wing micro aerial vehicle *2012 IEEE/RSJ Int. Conf. on Intelligent Robots and Systems* (IEEE) pp 126–31
[19] Howell L L 2013 Compliant mechanisms *21st Century Kinematics: The 2012 NSF Workshop* (Springer) pp 189–216
[20] Boyraz P, Runge G and Raatz A 2018 *Actuators* **7** 48
[21] Doyle C E, Bird J J, Isom T A, Kallman J C, Bareiss D F, Dunlop D J, King R J, Abbott J J and Minor M A 2012 *IEEE/ASME Trans. Mechatronics* **18** 506–17
[22] Ubellacker S, Ray A, Bern J, Strader J and Carlone L 2023 Aggressive aerial grasping using a soft drone with onboard perception preprint (arXiv:2308.06351)
[23] Zheng L and Hamaza S 2024 *IEEE Robot. Autom. Lett.* **9** 2845–52
[24] Landon S D, Magleby S P and Howell L L 2005 Preliminary concepts for deployable wings on small UAVs using compliance *ASME Int. Mechanical Engineering Congress and Exposition* vol 4210 (ASME) pp 353–63
[25] Xu K and Liu H 2022 *IEEE/ASME Trans. Mechatronics* **27** 5197–207
[26] Zhang C and Rossi C 2017 *Bioinspir. Biomim.* **12** 025005
[27] Sharifzadeh M and Aukes D M 2020 *IEEE/ASME Trans. Mechatronics* **26** 503–14
[28] Carollo G, Ingrassia T and Pantano A 2022 Design of a low-cost 3D printable single-component compliant mechanism for FWMAV's wing actuation *Design Tools and Methods in Industrial Engineering II* (Springer) pp 39–49
[29] Finio B M, Whitney J P and Wood R J 2010 Stroke plane deviation for a microrobotic fly *2010 IEEE/RSJ Int. Conf. on Intelligent Robots and Systems* (IEEE) pp 3378–85
[30] Chattaraj N and Ganguli R 2023 *Int. J. Aeronaut. Space Sci.* **24** 105–20
[31] Farhadi D, Tolou N and Herder J 2015 *J. Mech. Des.* **137** 032301
[32] Jensen B D and Howell L L 2002 *Mech. Mach. Theory* **37** 461–76
[33] JPE-Innovations 2022 Cross spring pivot construction fundamentals (available at: https://www.jpe-innovations.com/precision-point/cross-spring-pivot/) (Accessed 09 December 2025)
[34] Zhao L, Huang Q, Deng X and Sane S P 2009 *J. R. Soc. Interface* **7** 485–97
[35] Mrázek J 2022 Testing siraya tech fast mecha: a (r)evolution in functional 3D printing? (available at: https://blog.honzamrazek.cz/2022/02/testing-siraya-tech-fast-mecha-a-revolution-in-functional-3d-printing/) (Accessed 09 December 2025)
[36] Polymers P 2021 Technical datasheet – prusament tough resin (all colors) (available at: https://prusament.com/wp-content/uploads/2021/09/prusament_resin_tough_TDS_EN.pdf) (Accessed 09 December 2025)
[37] Photocentric 2025 Photocentric 1kg black flexible daylight resin (available at: https://www.cuttingandabrasives.com/product/photocentric-1kg-black-flexible-daylight-resin/) (Accessed 09 December 2025)
[38] Zortrax 2018 Technical datasheet – zortrax resin flexible (available at: https://zortrax.com/wp-content/uploads/2018/11/Zortrax_Resin_Flexible_Technical_Data_Sheet_eng.pdf) (Accessed 09 December 2025)
[39] Tech S 2025 Technical datasheet – siraya tech fast mecha white (available at: https://drive.google.com/file/d/1YonFvYVKbtiNLFdTRl_CQzqsFlzCtCCm/view) (Accessed 09 December 2025)
[40] Anycubic 2025 Anycubic colored UV resin (available at: https://store.anycubic.com/products/colored-uv-resin) (Accessed 09 December 2025)
[41] Phrozen 2025 Phrozen resin user guide (available at: https://filament2print.com/en/index.php?controller = attachment&id_attachment = 2330) (Accessed 09 December 2025)
[42] Caetano J V, Percin M, Van Oudheusden B W, Remes B, De Wagter C, De Croon G C H E and De Visser C C 2015 *Bioinspir. Biomim.* **10** 056004
[43] Thompson M, Watkins S, White C and Holmes J 2011 *Aeronaut. J.* **115** 693–701
[44] Kuresangsai P, Cole M O and Hao G 2024 *Mech. Mach. Theory* **202** 105779
[45] Howell L L, Magleby S P and Olsen B M 2013 *Handbook of Compliant Mechanisms* (Wiley)